Acta Crystallographica Section A
Foundations of Crystallography
ISSN 0108-7673

Received 2 April 2002
Accepted 28 August 2002

The generalized *F* constraint in the maximum-entropy method – a study on simulated data

Lukáš Palatinus* and Sander van Smaalen

Laboratory of Crystallography, University of Bayreuth, Germany. Correspondence e-mail: palat@uni-bayreuth.de

One of the classical problems in the application of the maximum-entropy method (MEM) to electron-density reconstructions is the uneven distribution of the normalized residuals of the structure factors $[|F_{\rm obs}(\mathbf{H})| - |F_{\rm calc}(\mathbf{H})|]/\sigma(\mathbf{H})$ of the resulting electron density. This distribution does not correspond to the expected Gaussian distribution and it leads to erroneous features in the MEM reconstructions. It is shown that the classical χ^2 constraint is only one of many possible constraints, and that it is too weak to restrict the resulting distribution to the expected Gaussian shape. It is proposed that constraints should be used that are based on the higher-order central moments of the distribution of the structure-factor residuals. In this work, the influence of different constraints on the quality of the MEM reconstruction is investigated. It is proposed that the use of a combined constraint on more than one central moment simultaneously would lead to again improved results. Oxalic acid dihydrate was chosen as model structure, from which several data sets with different resolutions and different levels of noise were calculated and subsequently used in the MEM. The results clearly show that the use of different constraints leads to significantly improved results.

1. Introduction

The maximum-entropy method (MEM) is used as a powerful tool for a model-free image reconstruction in many scientific applications (von der Linden *et al.*, 1998). In crystallography, one particular application is the investigation of the electron density in the crystal structure. After the first promising applications in this field (Collins, 1982; Sakata & Sato, 1990), several warnings concerning the reliability and possible pathologies of the method appeared (Jauch, 1994; de Vries *et al.*, 1996). One of the obvious problems was that the distribution of the normalized residuals of the structure factors $\Delta F(\mathbf{H})/\sigma(\mathbf{H}) = [|F_{\rm obs}(\mathbf{H})| - |F_{\rm calc}(\mathbf{H})|]/\sigma(\mathbf{H})$ strongly deviated from the expected Gaussian distribution. Some of the reflections – usually strong reflections at low angles – had very large $\Delta F(\mathbf{H})/\sigma(\mathbf{H})$, while the others were fitted almost exactly. The large deviation of the histogram of $\Delta F(\mathbf{H})/\sigma(\mathbf{H})$ from the Gaussian distribution was responsible for unphysical features in the corresponding electron density. A solution to this problem was proposed by de Vries *et al.* (1994), who employed an *ad hoc* weighting scheme within the classical χ^2 constraint. However, a theoretical basis for this weighting scheme does not exist.

Here we propose new constraints based on the higher-order central moments of the distribution of $\Delta F(\mathbf{H})/\sigma(\mathbf{H})$. We show that the use of these constraints produces results with better distributions of $\Delta F(\mathbf{H})/\sigma(\mathbf{H})$ and with less artifacts in the reconstructed electron density than the classical χ^2 constraint.

The method is tested against data sets of various resolutions and with various noise levels that were computed for a known electron density of oxalic acid dihydrate.

2. The method

The basic principle of the MEM is that the optimal image is defined to be the image with the maximum value of the entropy functional S, while one or more constraints of the type $C_j = 0$ $(j = 1, \ldots, N_c)$ are fulfilled. For our purposes, the image is the electron density (ρ) in the unit cell, which is defined by its values ρ_i on a grid of $N_p = N_1 \times N_2 \times N_3$ points. The entropy is defined as

$$S = -\sum_{i=1}^{N_p} \rho_i \log(\rho_i/\tau_i), \qquad (1)$$

where the values τ_i define the prior or reference electron density. For an overview of the crystallographic applications of the MEM, see Gilmore (1996). The constraints should be selected so as to define which image is in agreement with the observed data. The first reasonable constraint is the normalization of ρ to the expected number of electrons per unit-cell volume:

$$\int_V \rho \, {\rm d}V - N_{\rm el} = 0. \qquad (2)$$

Traditionally, the constraint to the scattering data is the least-squares likelihood criterion $\chi^2 - 1 = 0$, with

$$\chi^2 = \frac{1}{N_F}\sum_{i=1}^{N_F}\left(\frac{|F^i_{\rm obs}(\mathbf{H})| - |F^i_{\rm MEM}(\mathbf{H})|}{\sigma^i(\mathbf{H})}\right)^2, \quad (3)$$

where the summation runs over all measured structure factors N_F. This definition of the constraint cannot be used directly, since it does not contain the information about the phases of the structure factors and does not lead to convergence. Therefore, the so-called F constraint is usually employed:

$$C_F = -1 + \frac{1}{N_F}\sum_{i=1}^{N_F}\left(\frac{|F^i_{\rm obs}(\mathbf{H}) - F^i_{\rm MEM}(\mathbf{H})|}{\sigma^i(\mathbf{H})}\right)^2. \quad (4)$$

The value of C_F depends on both the amplitudes and phases of $F_{\rm obs}$ and $F_{\rm MEM}$. C_F is minimal if the phases of all $F^i_{\rm obs}$ are equal to the corresponding $F^i_{\rm MEM}$. In that case, $C_F = \chi^2 - 1$.

The use of the χ^2 statistics (and its phased modification in the C_F constraint) is based on an assumption that the experimental errors on $|F_{\rm obs}|$ are random with a Gaussian distribution:

$$\frac{|F_{\rm obs}(\mathbf{H})| - |F_{\rm true}(\mathbf{H})|}{\sigma(\mathbf{H})} = \varepsilon_{\rm Gauss}, \quad (5)$$

where $\varepsilon_{\rm Gauss}$ is a sample of the random variable with normalized Gaussian distribution. Since the resulting electron density $\rho_{\rm MEM}$ should be the best estimate of the true density, the corresponding calculated structure factors $F_{\rm MEM}$ should be the best estimate of $F_{\rm true}$ and the distribution of the normalized residuals should be Gaussian too.

It is obvious that the Gaussian distribution of errors does imply the validity of the χ^2 (or C_F) constraint, but not *vice versa*. Constraining only χ^2 is not sufficient to ensure the proper Gaussian form of the resulting error distribution.

A probability distribution of a random variable x is characterized by the values of its central moments m_n. For the normalized Gaussian distribution, the central moments are

$$m_n(\text{Gauss}) = \int_{-\infty}^{\infty} x^n (2\pi)^{-1/2}\exp(-x^2/2)\,{\rm d}x. \quad (6)$$

The values of the moments of odd order are all zero and the moments of even order are:

$$m_{2k}(\text{Gauss}) = \prod_{i=1}^{k}(2i-1). \quad (7)$$

In the case of N samples of the variable x, the central moments m_n can be computed from

$$m_n = (1/N)\sum_N x_i^n. \quad (8)$$

It follows from (3) and (8) that χ^2 is the m_2 central moment of the distribution of $\Delta F(\mathbf{H})/\sigma(\mathbf{H})$. Thus, the concept of generalized F constraint can be introduced, with F_2 referring to the classical constraint on the second-order moment, and with F_n defining a constraint based on the moment of order n:

$$C_{F_n} = -1 + \frac{1}{m_n(\text{Gauss})}\frac{1}{N_F}\sum_{i=1}^{N_F}\left(\frac{|F^i_{\rm obs}(\mathbf{H}) - F^i_{\rm MEM}(\mathbf{H})|}{\sigma^i(\mathbf{H})}\right)^n. \quad (9)$$

Table 1
Basic characteristics of the structure of oxalic acid dihydrate.

Chemical formula	HOOC—COOH·2H$_2$O
Chemical formula weight	126.06
Cell setting, space group	Monoclinic, unique axis b, $P2_1/n$
a, b, c (Å)	6.101, 3.500, 11.955
β (°)	105.78
V (Å^3)	245.64
Z	2

Only the constraints with n even restrict the width of the histogram, constraints with n odd are sensitive only to the symmetry of the distribution with respect to the origin. Therefore, only the constraints with n even are used in this work.

It has been suggested that more simultaneous constraints (up to the number of independent observations) of the form $[|F_{\rm obs}(\mathbf{H})| - |F_{\rm calc}(\mathbf{H})|]/\sigma(\mathbf{H})$ could be used instead of the single χ^2 constraint (Carvalho *et al.*, 1996). This requires some additional criterion for defining the point of convergence and strongly restricts the role of the MEM as the noise filter. We suggest that the use of several F_n constraints simultaneously is the proper way to handle noisy data, since the expected shape of the histogram is the only information about the noise that is available. However, the available algorithms do not allow such a generalization. Therefore, in the present stage of the work, the influence of different choices of a single constraint based on (9) on the result of MEM was investigated.

3. Computational details

The method was tested on the structure of oxalic acid dihydrate. The main reason for this choice was that this compound has become a kind of standard for charge-density studies. In addition, the structure of oxalic acid dihydrate is very suitable for this type of work, since it is centrosymmetric and the central molecule is planar. This allows an easy interpretation of the majority of the features using only one section of the electron density. The basic characteristics of the structure are summarized in Table 1.

First, the electron density of the procrystal structure (superposition of independent atoms, $\rho_{\rm pro}$) was created. This was done by a method due to Papoular *et al.* (2002). The analytical approximation to spherical atomic scattering factors (Su & Coppens, 1997) for each atom of the structure was multiplied by the anisotropic displacement factor of that atom. The resulting three-dimensional distribution in reciprocal space was then transformed by means of the analytical Fourier transform to obtain the electron density of that atom. The density was sampled on the $64 \times 32 \times 128$ pixel grid, which corresponds to a pixel size of approximately $0.1 \times 0.1 \times 0.1$ Å. The positional and displacement parameters from the refinement due to Šlouf (2001) were used. The electron densities of the individual atoms were then summed to obtain $\rho_{\rm pro}$. The 'true' electron density $\rho_{\rm true}$ was then constructed by summing $\rho_{\rm pro}$ with the dynamic deformation density $\rho_{\rm def}$, as determined by the multipole refinement of

Šlouf (2001) (Fig. 1*a*). This caused 1.65% of the pixels of the resulting electron density to be negative. The lowest density was −0.021 e Å^{-3}. The negative areas were located in the low-density intermolecular regions. This unphysical feature probably originates from the inaccuracy of the multipole expansion in these very low density regions. The MEM cannot handle these negative regions and very low density regions increase the dynamic ratio of the electron density inadequately. Therefore, the pixels with $\rho < 0.005$ e Å^{-3} were set to 0.005 e Å^{-3}. 2.45% of the pixels were corrected.

The electron density obtained by this procedure is certainly not the true electron density of oxalic acid dihydrate. The analytical approximation used in the first step is not absolutely accurate and the structure parameters and multipole deformation density can contain a substantial degree of inaccuracy, too. However, this model of electron density is good enough to be used as the reference electron density for MaxEnt calculations and will be denoted as $\rho_{\rm true}$ (Fig. 1*b*).

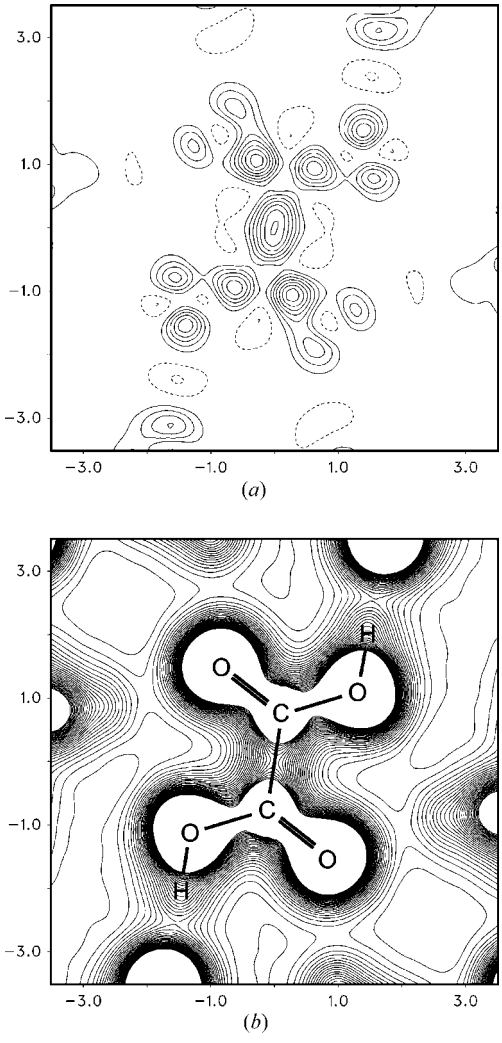

Figure 1
The sections of the true electron density showing the oxalic acid molecule. (*a*) The dynamic deformation density $\rho_{\rm def}$ obtained by the multipole refinement (Šlouf, 2001). (*b*) The total electron density $\rho_{\rm true}$. Scale in Å, contours 0.07 e Å^{-3}, cut-off 2.0 e Å^{-3}, zero contour omitted. Maximum of the deformation density 0.56 e Å^{-3}, maximum of the total density 56.79 e Å^{-3}.

The structure factors corresponding to the original map were calculated by means of a numerical Fourier transform. To investigate the influence of noise and resolution on the quality of the MEM reconstruction, 16 different data sets were created. The value $(\sin\Theta/\lambda)_{\rm max}$ is used as a measure of resolution in this paper. It was chosen to be 0.5, 0.75, 1.0 and 1.25 Å^{-1} for the respective data sets, and for each resolution four different levels of Gaussian noise were added to the calculated structure factors. To simulate the error distribution in real experimental data, $\sigma(F_{\rm obs})$ were calculated from

$$\sigma(F_{\rm obs}) = \nu[p|F_{\rm obs}|^2 + (\beta + |F_{\rm obs}|^2)/|F_{\rm obs}|^2]^{1/2}, \qquad (10)$$

where ν defines the noise level, β simulates the influence of non-zero background and p is the commonly used instability factor. The noisy 'observed' structure factors were then calculated to fulfil the equation

$$F_{\rm obs} = F_{\rm true} + \sigma(F_{\rm obs})\varepsilon_{\rm Gauss}. \qquad (11)$$

Here, $\varepsilon_{\rm Gauss}$ is a random variable with normalized Gaussian probability distribution. Three different non-zero noise levels were created this way. The noiseless data sets at each resolution were included for checking purposes. Although the structure factors in the noiseless data sets were exact, which means they should be assigned a zero standard deviation, this is not possible owing to the nature of the constraints [equation (9)]. Therefore, the value of $\sigma(F_{\rm obs})$ was set to 0.005 for all structure factors so as to be low enough and to allow the computations to finish in a reasonable time. The parameters of different noise levels and resolutions are summarized in Table 2 and Fig. 2.

It is interesting to compare the phases of structure factors corresponding to $\rho_{\rm true}$ with the phases corresponding to $\rho_{\rm pro}$. In the present case, which is representative for investigations of accurate electron densities, the amount of the unknown structure is minute and the phases of the true structure factors are very well estimated by the phases of the structure factors of $\rho_{\rm pro}$. Among all 4029 structure factors, up to $(\sin\Theta/\lambda)_{\rm max} = 1.25$ Å^{-1}, only nine have different phases for $\rho_{\rm true}$ and $\rho_{\rm pro}$. Moreover, equation (11) allows for changes of phases between $F_{\rm obs}$ and $F_{\rm true}$. As a consequence of the introduction of the noise, there have been many more phases changed in each noisy data set than nine. Thus, the results presented here are not influenced by the preliminary multipole refinement and can be regarded as being obtained using just the standard refinement.

We have developed our own computer program *BayMEM* (first version by Schneider, 2001) for the application of the MEM in charge-density analysis. This program is designed to work in general *n*-dimensional space to allow computations of the MEM electron density of incommensurately modulated structures, but can be used for standard three-dimensional structures too without any restrictions. *BayMEM* can use both the algorithm of Sakata & Sato (1990) and the *MEMSys5* package (Gull & Skilling, 1999). The program was extended to

Table 2
Parameters of the data sets.

Reflections with $|F_{obs}| < 5\sigma(F_{obs})$ [which corresponds to $I < 2.5\sigma(I)$] are considered unobserved. The shorthand notation used in text and figures for a given data set consists of the letter n and the noise level followed by the letter r and the value of $(\sin\Theta/\lambda)_{max}$ of the resolution. For example, n1r0.75 denotes data set with noise level 1 and resolution $(\sin\Theta/\lambda)_{max} = 0.75$ Å^{-1}. For definitions of ν, β and p, see equation (10).

Noise levels

	Level 0	Level 1	Level 2	Level 3
ν	0.005	0.025	0.1	0.25
β	0	1	10	15
p	0	0.0001	0.0001	0.0001

Resolution

Shells in $\sin\Theta/\lambda$ (Å^{-1})	Independent reflections	Observed/unobserved		
		Level 1	Level 2	Level 3
<0, 0.5>	258	253/5	235/23	217/41
(0.5, 0.75>	608	574/34	468/140	358/250
(0.75, 1.00>	1182	1042/140	714/468	425/757
(1.00, 1.25>	1981	1480/501	604/1377	165/1816

deal with the generalized F constraint. For the present study, the algorithm by Sakata & Sato (1990) was used.

The following characteristics are used to compare the quality of the *MaxEnt* reconstructions:

(i) the values of the even central moments of the distribution of normalized residuals;

(ii) the overall shape of the histogram;

(iii) the section through ρ_{MEM} in the plane of the HOOC—COOH molecule;

(iv) the section through the difference map $\rho_{diff} = \rho_{MEM} - \rho_{true}$ in the plane of the HOOC—COOH molecule;

(v) the MEM deformation density $\rho_{MEM-pro} = \rho_{MEM} - \rho_{pro}$ in the plane of the HOOC—COOH molecule;

(vi) the coincidence factor C, which allows for an easy comparison among different reconstructions by one number:

$$C = \sum_{i=1}^{N_p} |\rho^i_{MEM} - \rho^i_{true}| \Big/ \sum_{i=1}^{N_p} \rho^i_{true}. \qquad (12)$$

For all n1, n2 and n3 data sets, the computations using the F_n constraints of order 2 to 8 were performed, for the n0 data set only the orders 2 to 6 were used, since there was no visible influence of the constraint on the results. For comparison, the computations using the *ad hoc* weighting (de Vries *et al.*, 1996, referred to as static weighting hereafter) were performed on the noisy data sets. The F constraint with additional static weighting is defined as

$$C_w = -1 + \frac{1}{N_F} \sum_{i=1}^{N_F} w(F_{obs}) \left(\frac{|F^i_{obs}(\mathbf{H}) - F^i_{calc}(\mathbf{H})|}{\sigma^i(\mathbf{H})} \right)^2. \qquad (13)$$

Weights of the form $w = 1/|\mathbf{H}|^n$ ($|\mathbf{H}|$ is the length of the diffraction vector) with n equal to 3, 4 and 5 were used in this work. To investigate the influence of the prior electron density, two series of calculations were performed. The first series was made with the uniform prior, the second series with the procrystal prior ρ_{pro}.

The quality of the MEM reconstructions can be compared with Fourier maps. The Fourier transform of the observed structure factors with calculated phases results in an electron density (ρ_{fou}) that can be compared with ρ_{MEM} as obtained with the uniform prior. Inspection of ρ_{fou} shows that the noise is much larger than in ρ_{MEM}. This is quantified by the C values (Table 4).

The classical method to derive information about electron densities beyond the model is the difference Fourier. We have computed the difference Fourier for $F_{obs} - F_{pro}$ (ρ_{df}). To be able to compare the result with ρ_{MEM}, we have added ρ_{pro} to ρ_{df}. Again, the noise in $\rho_{fou} + \rho_{df}$ is significantly larger than in ρ_{MEM} (Table 5).

4. Results and discussion

4.1. The uniform prior

In the first series of calculations, a uniform electron density was used as prior. The dominating structure of ρ_{diff} is the oscillatory electron density around each atomic position (Fig. 3). Its presence is independent of the constraint and of the noise level. However, at high noise levels these features are partly camouflaged by the noise of ρ_{MEM} itself. The oscillations are most pronounced at the zero noise level. Clearly, this effect is a demonstration of the series-termination error intrinsically present in the method, as pointed out already by

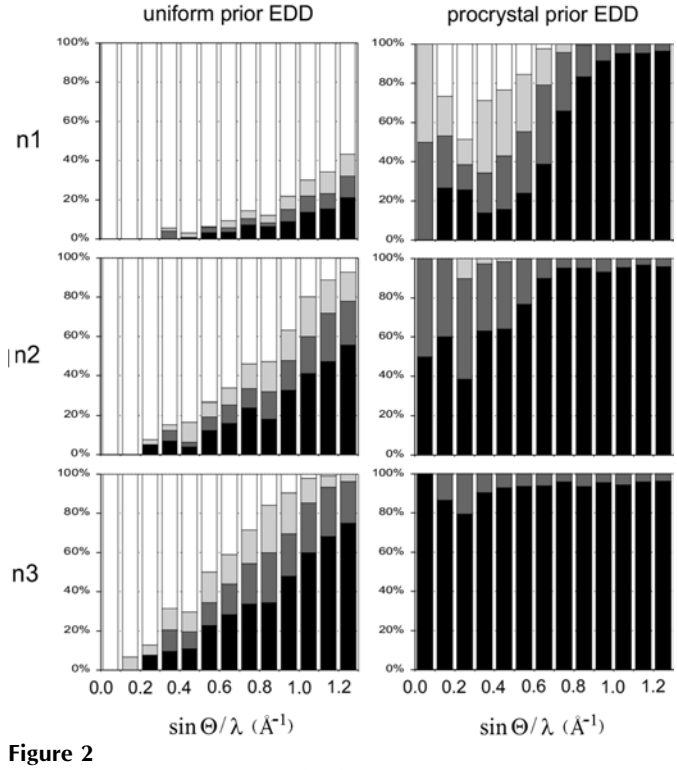

Figure 2
Distribution of $|F_{obs} - F_{prior}|/\sigma(F_{obs})$ as a function of the resolution for different noise levels. Note that for uniform prior $F_{prior} = 0$ for all structure factors except $F(000)$. Black: $\Delta F < 2\sigma$; dark gray: $2\sigma < \Delta F < 5\sigma$; light gray: $5\sigma < \Delta F < 10\sigma$; white: $10\sigma < \Delta F$.

Table 3
Extremals of the artifacts at different resolutions for n0 noise level and F_2 constraint.

	max	min
r0.50	4.36	−28.62
r0.75	3.32	−10.87
r1.00	4.94	−1.84
r1.25	3.42	−0.95

Jauch (1994) and later discussed in detail by Roversi *et al.* (1998). The present results show the extent of this effect and its dependence on the resolution of the data set. The amplitude of the artifacts ($\rho_{\rm diff}^{\rm max} - \rho_{\rm diff}^{\rm min}$) decreases with resolution, but even at resolution 1.25 Å remains significant (Fig. 3, Table 3). Further lowering of the artifacts by increasing the resolution is in practice not possible due to the experimental limitations. Possible ways to overcome this problem are summarized in §5.

The $\rho_{\rm MEM}$ obtained for different noise levels and different resolutions is characterized by the C values (Table 4), by the shapes of the histograms of $\Delta F(\mathbf{H})/\sigma(\mathbf{H})$ (Fig. 4), and by the values of the central moments of the distribution of $\Delta F(\mathbf{H})/\sigma(\mathbf{H})$ (Fig. 5). The following conclusions can be made based upon the table and the figures:

(i) The use of the higher-order constraints significantly improves the quality of $\rho_{\rm MEM}$. The improvement is largest between the F_2 and F_4 constraints. Only for the noiseless data sets does the use of different constraints not have any effect on the resulting C value, although the effect on the histogram is large. This is because at this noise level the C value is determined mainly by the series-termination artifacts, which are almost independent of the particular constraint. The improvement is generally better with increasing resolution. The probable reason for this is not the higher resolution itself but rather the higher number of reflections in the data set.

(ii) The histograms of the higher-order constraints are much closer to the ideal Gaussian distribution than the F_2 histograms and the number of very large normalized residuals is reduced (Fig. 4). On the other hand, these histograms are not free of systematic errors either. The histograms of the higher-order constraints tend to be slightly asymmetric towards positive differences. For a smaller number of reflections and/or lower noise level, the histograms tend to have a flatter peak with respect to the ideal shape and in the extreme case split into two distinct peaks (Fig. 4). The two peaks tend to be at the positions $\pm[m_n(\text{Gauss})]^{1/n}$, which correspond to the average value of normalized residual necessary to fulfil the given constraint. This is not the exclusive property of higher-order

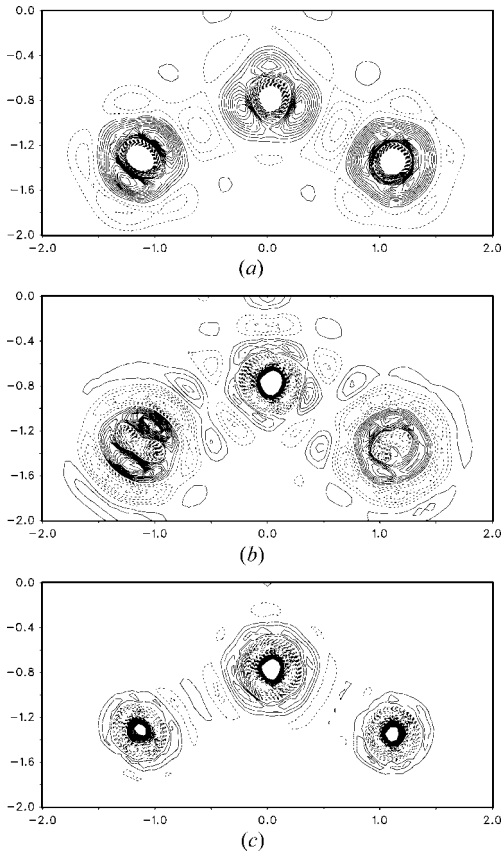

Figure 3
Sections through the difference electron-density map $\rho_{\rm diff}$ showing one COOH group. Uniform prior. (*a*) n0r0.75, contours 0.2 e Å^{-3}, cut-off 3.0 e Å^{-3}. (*b*) n0r1.00, contours 0.05 e Å^{-3}, cut-off 1.0 e Å^{-3}. (*c*) n0r1.25, contours as in (*b*). The decreasing width of the waves of the difference density with increasing resolution and the interference of the waves is clearly visible.

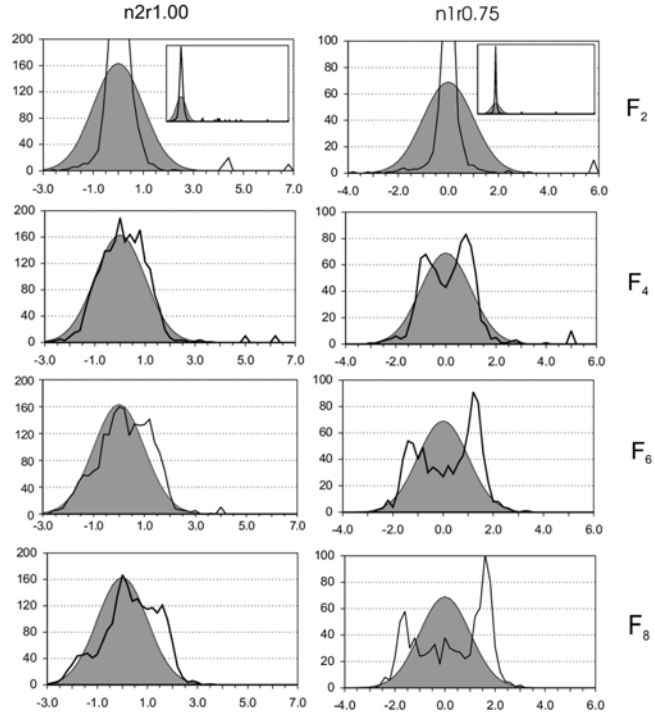

Figure 4
The histograms of $\Delta F(\mathbf{H})/\sigma(\mathbf{H})$ for different constraints. Uniform prior. For the F_2 histograms, only the central section is shown for good comparability; the full histogram is shown in the inset. The ideal Gaussian shape is shown as the grey area in each histogram. The counts of normalized residuals in classes higher than 4.0 are multiplied by 10.

Table 4
The coincidence factors $C = \sum_{i=1}^{N_p} |\rho_i^{\rm MEM} - \rho_i^{\rm true}| / \sum_{i=1}^{N_p} \rho_i^{\rm true}$ for MaxEnt calculations using the uniform prior and $\rho_{\rm fou}$.

F_n denotes the generalized F constraint of order n, sw$n$ denotes the static weighting with weight $w = 1/|H|^n$ [for definition see equation (13), for definition of shorthand notation of different data sets see Table 2]. *Note:* Some calculations could not be finished using the algorithm of Sakata & Sato (1990) due to convergence problems. For static weighting computations, this could be overcome by using the *MEMSys5* package (Gull & Skilling, 1999). These results are shown in italic. Generally, the differences between the results of the two algorithms are not very large, but the results of the latter algorithm seem to be slightly better. The calculation with the F_6 constraint on the n0r0.50 data set did not converge (denoted by n.c.).

Data set	F_2	F_4	F_6	F_8	sw3	sw4	sw5	$\rho_{\rm fou}$
n3r0.50	0.3515	0.2971	0.2942	0.2961	0.2884	0.2631	0.2548	1.3375
n3r0.75	0.3455	0.2237	0.2180	0.2230	0.1836	0.1546	0.1567	1.2187
n3r1.00	0.4137	0.2021	0.1873	0.1885	0.1569	0.1119	0.1179	1.1329
n3r1.25	0.4880	0.2316	0.1976	0.1970	0.1709	0.1073	0.1046	1.1434
n2r0.50	0.2730	0.2498	0.2515	0.2539	0.2447	0.2353	0.2326	1.3323
n2r0.75	0.2126	0.1476	0.1469	0.1502	0.1359	0.1212	*0.1209*	1.2073
n2r1.00	0.2250	0.1059	0.1010	0.1033	0.0935	0.0661	*0.0685*	1.1000
n2r1.25	0.2755	0.1063	0.0967	0.0969	0.1018	0.0632	0.0629	1.0440
n1r0.50	0.2287	0.2250	0.2254	0.2260	0.2233	0.2221	0.2457	1.3290
n1r0.75	0.1186	0.1026	0.1026	0.1033	0.1017	0.0998	0.1303	1.2061
n1r1.00	0.0815	0.0458	0.0448	0.0456	0.0451	0.0382	0.0708	1.0977
n1r1.25	0.0952	0.0365	0.0343	0.0353	0.0355	0.0255	0.0247	1.0339
n0r0.50	0.2199	0.2199	n.c.					
n0r0.75	0.0949	0.0949	0.0950					
n0r1.00	0.0286	0.0289	0.0290					
n0r1.25	0.0147	0.0151	0.0155					

constraints, similar splitting can appear in the F_2 histograms, too, although only in very extreme cases (n0r0.50).

(iii) The quality of the result (measured by the C value) is perfectly correlated with the quality of the histogram expressed by the values of its central moments. The best results are obtained with that constraint, which produces a histogram closest to the expected normalized Gaussian (compare Table 4 and Fig. 5). With increasing order of the constraint, the resulting histograms get better first (the large positive slope of the curve in Fig. 5 gets smaller) and then the high-order central moments of the histograms become overestimated (the slope of the curves in Fig. 5 becomes negative). The best result is obtained when the slope of the curve is close to zero. We suggest that, if there are two constraints close to the optimal slope, the one with positive slope should be preferred. This can be understood to be a choice between slightly underestimating and slightly overestimating the data. Using the constraint with positive slope means possibly losing some information present in the data, using the one with negative slope means letting the MEM fit some noise and thus introducing some false features in the resulting $\rho_{\rm MEM}$. But in practice the difference between the two results is negligible.

The improvement of the $\rho_{\rm MEM}$ is visible in both the total and difference electron-density maps $\rho_{\rm MEM}$ and $\rho_{\rm diff}$ (Fig. 6). The waviness of the low-density contours in $\rho_{\rm MEM}$ is suppressed, the overall amount of the residual structure in $\rho_{\rm diff}$ decreases. It should be noted that the total density maps do not give sufficient insight into the accuracy of the result and cannot be used as a single criterion of the quality of the *MaxEnt* reconstruction. This can be seen from the comparison of the total and difference maps (Fig. 6). The largest errors occur in the medium and high density levels, where the total density map seems to be smooth and well behaved. This is especially true for the low-resolution maps, which seem to be smooth at first sight, but which exhibit large differences in comparison to the original map.

Despite the significant improvement of the MEM reconstructions obtained with the constraints on the higher-order moments, the quality of the reconstructions using the static weighting was in our case even better (Table 4). This

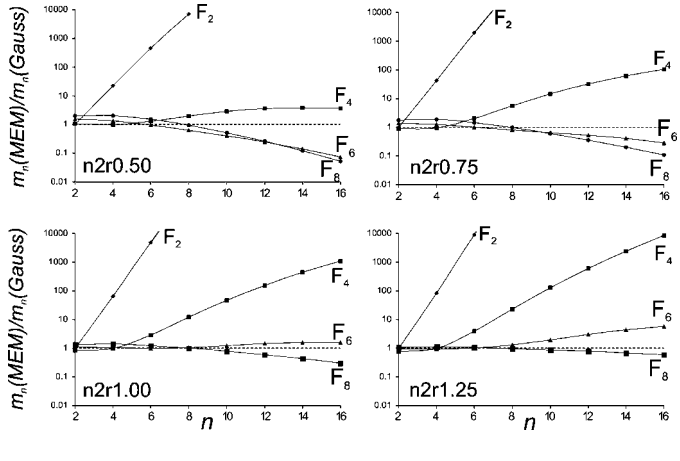

Figure 5
The even central moments m_2 to m_{16} of the histograms of all MEM runs on the n2 data sets. Uniform prior. Horizontal axis = order of the moment, vertical axis = normalized values of the moments m_n(MEM)/m_n(Gauss) on a logarithmic scale. Each curve corresponds to one histogram and is labeled with the constraint used for the MaxEnt calculation.

surprising effectiveness of the idea of the static weighting suggests that there might exist some fundamental reason for it. A closer investigation of possible theoretical foundations of this type of weighting is desirable.

The systematic investigation of the large number of different data sets allows one to make some general conclusions about the influence of the noise and the resolution on the quality of the result. The expected improvement of the C factors with decreasing noise level is clearly visible. The improvement with the increasing resolution is visible, too, but not as an absolute rule (compare C values of n3r1.00 and n3r1.25, n2r1.00 and n2r1.25 in Table 4). This can be correlated with Fig. 2. The larger the fraction of unobserved reflections present in the outer shell, the smaller is the amount of information it contains. In the data sets with the high noise level, almost all reflections in the outer shells are less-than's, and they cannot contribute to the improvement of the MEM reconstruction.

4.2. The procrystal prior

In the second series of calculations, the procrystal electron density $\rho_{\rm pro}$ was used as prior. The summary of the resulting C values is given in Table 5. The deformation density $\rho_{\rm MEM} - \rho_{\rm pro}$ obtained with data sets n2r1.00 and n1r0.75 is shown in Fig. 7. We believe that these examples are quite close to the data sets obtainable in practice.

As expected, the artifacts are strongly reduced and visible only in the vicinity of the atomic center. The deformation density resembles the true deformation density quite well even for the medium noise level. The differences in C factors among the different F_n constraints and the different static weighting are much smaller than in the case of the uniform prior, but they are still significant, especially for the low noise levels.

With increasing noise level, the outer shells of structure factors contain so much noise that it masks their statistical

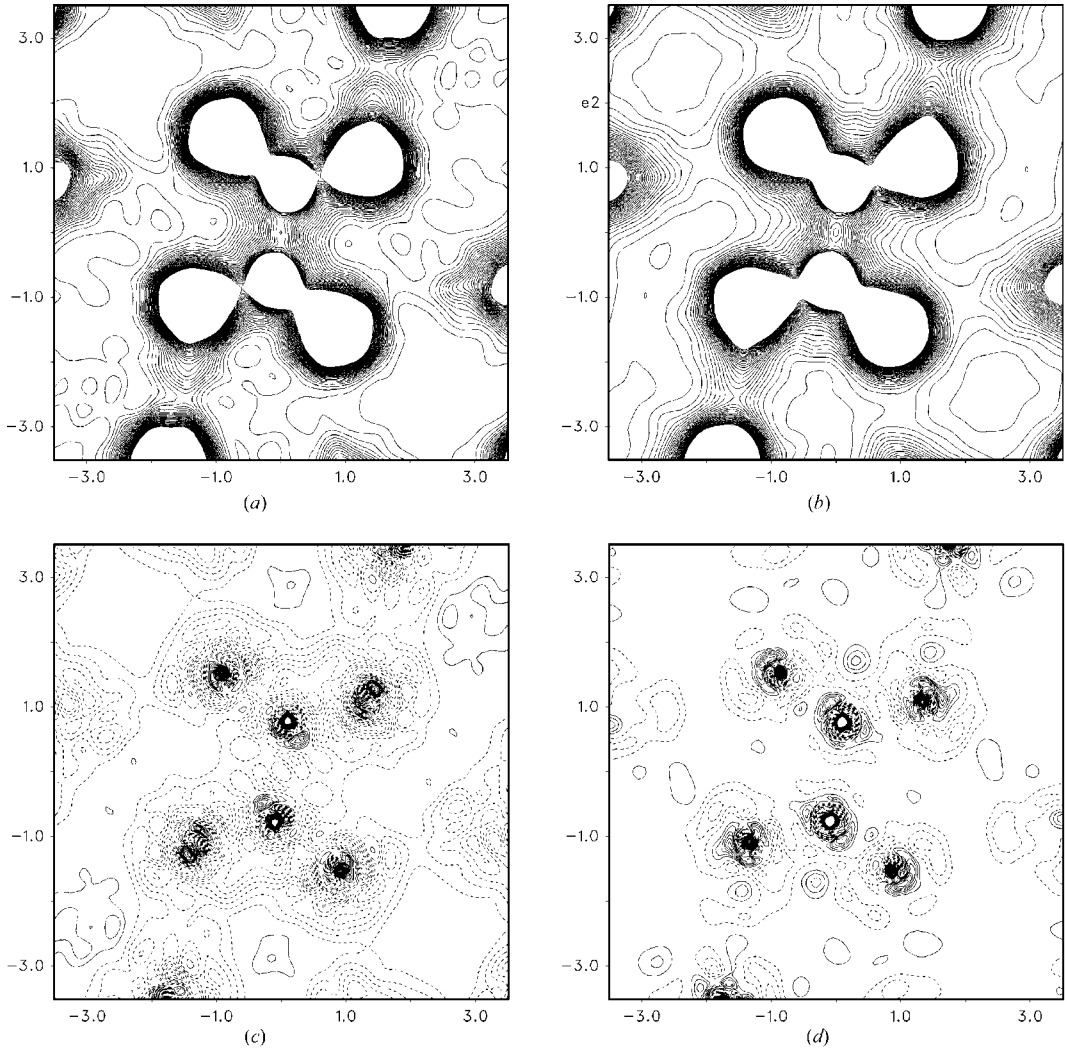

Figure 6
$\rho_{\rm MEM}$ and $\rho_{\rm diff}$ obtained with the n2r1.00 data set and with the uniform prior. (*a*) $\rho_{\rm MEM}$, F_2 constraint. (*b*) $\rho_{\rm MEM}$, F_6 constraint. (*c*) $\rho_{\rm diff}$, F_2 constraint. (*d*) $\rho_{\rm diff}$, F_6 constraint. All contours as in Fig. 1.

Table 5
The coincidence factors $C = \sum_{i=1}^{N_p} |\rho_i^{\rm MEM} - \rho_i^{\rm true}| / \sum_{i=1}^{N_p} \rho_i^{\rm true}$ for MaxEnt calculations using the procrystal prior and $\rho_{\rm pro} + \rho_{\rm df}$.

For explanation of the symbols see Table 4. The C factor of the procrystal prior is 0.0598.

Data set	F_2	F_4	F_6	F_8	sw3	sw4	sw5	$\rho_{\rm pro} + \rho_{\rm df}$
n3r0.50	0.0538	0.0560	0.0589	0.0585	0.0554	0.0574	*0.0575*	0.1015
n3r0.75	0.0554	0.0552	0.0580	0.0574	0.0534	*0.0513*	*0.0533*	0.2023
n3r1.00	0.0598	0.0597	0.0590	0.0592	0.0598	0.0598	*0.0545*	0.3308
n3r1.25	0.0598	0.0598	0.0598	0.0598	0.0598	0.0598	*0.0555*	0.4856
n2r0.50	0.0421	0.0423	0.0443	0.0458	0.0400	0.0403	*0.0386*	0.0598
n2r0.75	0.0434	0.0404	0.0414	0.0433	0.0361	0.0353	*0.0328*	0.1016
n2r1.00	0.0496	0.0447	0.0453	0.0466	0.0420	*0.0358*	*0.0372*	0.1744
n2r1.25	0.0545	0.0491	0.0486	0.0496	0.0483	0.0473	*0.0350*	0.2702
n1r0.50	0.0285	0.0259	0.0258	0.0262	0.0253	0.0248	*0.0236*	0.0340
n1r0.75	0.0275	0.0233	0.0219	0.0224	0.0209	0.0184	*0.0172*	0.0206
n1r1.00	0.0290	0.0220	0.0208	0.0211	0.0205	*0.0170*	*0.0157*	0.0339
n1r1.25	0.0321	0.0245	0.0229	0.0229	0.0218	*0.0174*	*0.0150*	0.0563
n0r0.50	0.0224	0.0223	0.0223					
n0r0.75	0.0106	0.0105	0.0104					
n0r1.00	0.0057	0.0056	0.0057					
n0r1.25	0.0038	0.0041	0.0045					

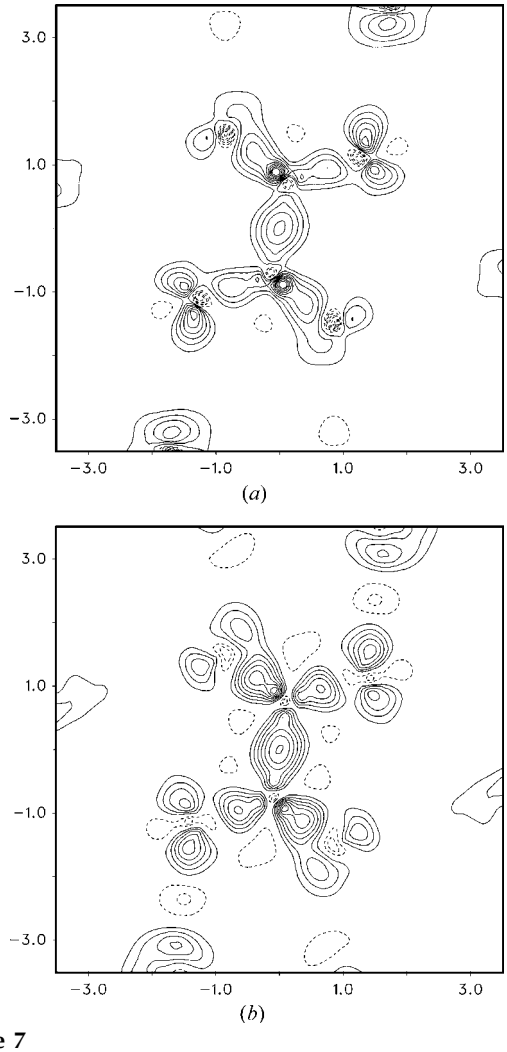

Figure 7
MEM deformation electron density, $\rho_{\rm MEM} - \rho_{\rm pro}$. Calculations with $\rho_{\rm pro}$ prior. (*a*) n2r0.75 data set, F_4 constraint. (*b*) n1r1.00 data set, F_6 constraint. All contours as in Fig. 1.

difference from the prior structure factors. Such reflections do not improve the result and can even lead to a slightly worse $\rho_{\rm MEM}$ (compare Table 5 and Fig. 2). In an extreme case – noise level 3 – the reflections do not provide any additional information at all and $\rho_{\rm MEM}$ is almost identical with the prior. In other words, the MEM indicates that the data do not contain any evidence for deviation from the prior.

The results confirm that, with procrystal prior information, the MEM is able to reveal the deformation electron density even from the medium-resolution data, provided they are sufficiently accurate.

5. Conclusions

The intrinsic presence of the series-termination effect in the crystallographic applications of the MEM is demonstrated. The extent of this effect depends on the resolution of the data set and on the kind of prior electron density. For the uniform prior, the artifacts are significantly higher than the bonding electron-density level and make this version of the MEM unsuitable for investigation of fine features in the electron density. Nevertheless, it is still a useful method for investigation of more robust features like anharmonic atomic movement or disorder (Bagautdinov *et al.*, 1998; Dinnebier *et al.*, 1999; Wang *et al.*, 2001).

The procrystal prior electron density lowers the artifacts and the reconstructions with this prior contain the information about the fine features of the electron density. Further lowering of the artifacts could probably be achieved with the two-channel MEM (Papoular *et al.*, 1996) or with the valence-only MEM proposed by Roversi *et al.* (1998). The latter method uses the refined structure parameters to create a core electron-density fragment, which is then considered to be known and is not included in the MaxEnt optimization. Only the valence electron density is modified. However, this

method is of practical use only for extremely accurate data from simple structures, since it relies on the knowledge of the temperature parameters, which are often inaccurate and correlated with systematic errors in the data sets.

The use of the generalized F constraint dramatically improves the quality of the MEM results. The selection criterion for the proper order is the best coincidence of the histogram with the expected Gaussian distribution. From our experience, the order 4 or 6 gives the best result.

Static weighting still gives better results than the non-weighted F_n constraints. But this type of weighting lacks any theoretical foundation, and the choice of the best weighting is very data set dependent (Yamamoto *et al.*, 1996). On the other hand, the constraints based on the expected moments of the distribution of $\Delta F(\mathbf{H})/\sigma(\mathbf{H})$ have a clear interpretation. One can expect that the new algorithms that will allow the simultaneous use of several constraints in the MEM will again lead to improved results.

One more advantage of the higher-order F constraints in comparison to the classical F_2 constraint or static weighting is faster convergence, which makes the computation time significantly shorter.

Financial support by the Deutsche Forschungsgemeinschaft is gratefully acknowledged.

References

Bagautdinov, B., Luedecke, J., Schneider, M. & van Smaalen, S. (1998). *Acta Cryst.* B**54**, 626–634.

Carvalho, C., Hashizume, H., Stevenson, A. & Robinson, I. (1996). *Physica (Utrecht)*, B**221**, 469–486.

Collins, D. M. (1982). *Nature (London)*, **298**, 49–51.

Dinnebier, R. E., Schneider, M., van Smaalen, S., Olbrich, F. & Behrens, U. (1999). *Acta Cryst.* B**55**, 35–44.

Gilmore, C. J. (1996). *Acta Cryst.* A**52**, 561–589.

Gull, S. F. & Skilling, J. (1999). *MemSys5 v1.2 Program Package.* Suffolk, United Kingdom.

Jauch, W. (1994). *Acta Cryst.* A**50**, 650–652.

Linden, W. von der, Dose, V., Fisher, R. & Preuss, R. (1998). Editors. *Maximum Entropy & Bayesian Methods.* Dordrecht: Kluwer Academic Publishers.

Papoular, R. J., Vekhter, Y. & Coppens, P. (1996). *Acta Cryst.* A**52**, 397–407.

Papoular, R. J., Collin, G., Colson, D. & Viallet, V. (2002). In *Proccedings of the 21st Workshop on Bayesian Inference and Maximum Entropy Methods in Science and Engineering*, edited by R. Fry. Melville, NY: American Institute of Physics. To be published.

Roversi, P., Irwin, J. J. & Bricogne, G. (1998). *Acta Cryst.* A**54**, 971–996.

Sakata, M. & Sato, M. (1990). *Acta Cryst.* A**46**, 263–270.

Schneider, M. (2001). PhD thesis, University of Bayreuth, Germany.

Šlouf, M. (2001). PhD Thesis, Charles University, Prague, Czech Republic.

Su, Z. & Coppens, P. (1997). *Acta Cryst.* A**53**, 749–762.

Vries, R. Y. de, Briels, W. J. & Feil, D. (1994). *Acta Cryst.* A**50**, 383–391.

Vries, R. Y. de, Briels, W. J. & Feil, D. (1996). *Phys. Rev. Let.* **77**, 1719–1722.

Wang, C.-R., Jai, T., Tomiyama, T., Yoshida, T., Kobayashi, Y., Nishibori, E., Takata, M., Sakata, M. & Shinohara, H. (2001). *Angew. Chem. Int. Ed. Engl.* **40/2**, 397–399.

Yamamoto, K., Takahashi, Y., Ohshima, K., Okamura, F. P. & Yukino, K. (1996). *Acta Cryst.* A**52**, 606–613.